Fingerprints of the Local Moment Formation and its Kondo Screening in the Generalized Susceptibilities of Many-Electron Problems

P. Chalupa,[1] T. Schäfer,[2,3] M. Reitner,[1] D. Springer,[1,4] S. Andergassen,[5] and A. Toschi[1]
[1]Institute of Solid State Physics, TU Wien, A-1040 Vienna, Austria
[2]Collège de France, 11 place Marcelin Berthelot, 75005 Paris, France
[3]CPHT, CNRS, École Polytechnique, Institut Polytechnique de Paris, Route de Saclay, 91128 Palaiseau, France
[4]Institute of Advanced Research in Artificial Intelligence, IARAI, A-1030 Vienna, Austria
[5]Institut für Theoretische Physik and Center for Quantum Science, Universität Tübingen, Auf der Morgenstelle 14, 72076 Tübingen, Germany

(Received 23 July 2020; revised 8 December 2020; accepted 8 January 2021; published 4 February 2021)

We identify the precise hallmarks of the local magnetic moment formation and its Kondo screening in the frequency structure of the generalized charge susceptibility. The sharpness of our identification even pinpoints an alternative criterion to determine the Kondo temperature of strongly correlated systems on the two-particle level, which only requires calculations at the *lowest* Matsubara frequency. We showcase its strength by applying it to the single impurity and the periodic Anderson model as well as to the Hubbard model. Our results represent a significant progress for the general understanding of quantum field theory at the two-particle level and allow for tracing the limits of the physics captured by perturbative approaches for correlated systems.

DOI: 10.1103/PhysRevLett.126.056403

Introduction.—The goal of any successful theory is to extract essential features of the phenomena of interest from the complexity of the physical world, neglecting all superfluous pieces of information. This objective is particularly crucial for the cutting-edge quantum field theory (QFT) approaches designed to describe many-electron systems in the presence of strong correlations.

Presently, one can rely on a solid textbook interpretation [1,2] of the QFT formalism describing the single-particle (1P) processes, measurable, e.g., by (angular resolved) direct and inverse photoemission [3] or scanning tunneling microscopy [4,5]. Crucial information about the metallic or insulating nature of a given many-electron problem, as well as quantitative information about the electronic mass renormalization Z and quasiparticle lifetime τ is encoded in the momentum and energy dependence of the electronic self-energy Σ. If the temperature T is low enough, even a quick glance at the low-energy behavior of Σ, either in real or in Matsubara frequencies, yields a qualitatively reliable estimate of the most important physical properties.

The situation is clearly different on the two-particle (2P) level, which can be experimentally accessed by, e.g., inelastic neutron scattering [6,7]. Because of the complex physical mechanisms at play, the related textbook knowledge is mostly limited to general definitions [1,2]. For this reason, corresponding analytical or numerical calculations are often performed with significant approximations or with a black-box treatment of the 2P processes. However, the last decade has seen a rapid development of methods at the forefront of the many-electron theory [8–10], for which generalized 2P correlation functions are the key ingredient. This is reflected in an increasing effort to develop the corresponding formal aspects and algorithmic procedures [8–31]. At the same time, the rather poor physical understanding of the 2P processes remains largely behind the requirements of the most advanced QFT methods. Interesting progress has been recently reported [32,33] on the relation of 1P Fermi-liquid parameters to 2P scattering functions. Ideally, however, one would like to be able to interpret the physics encoded at the 2P level with a similar degree of confidence as for the 1P processes.

In our Letter, we make a significant step forward in this direction: We identify the fingerprints of two major hallmarks of strong correlations in the generalized charge susceptibility. In particular, we pinpoint the frequency structures encoding the formation of local magnetic moments as well as of their Kondo screening. In this perspective, we also show how the Kondo temperature T_K corresponds to a specific property of the generalized charge susceptibility, allowing for an alternative, simple path of extracting its value directly from the lowest Matsubara frequency data.

We recall that the Kondo problem [34] provides a paradigm for a variety of physical effects [35–39] involving strong electronic correlations. Local moment formation and Kondo screening are also a crucial ingredient of the physics described by the dynamical mean-field theory (DMFT) [40] through the solution of a self-consistently determined auxiliary Anderson impurity model (AIM).

Learning how to extract important physical information from the generalized susceptibility represents a substantial improvement for the understanding of quantum many-electron physics at the 2P level. Further, having this information at hand also enables us to draw conclusions on two relevant theoretical questions: (i) The relation of the recently reported multifaceted manifestations [41] of the breakdown of perturbation theory, such as the divergences of the irreducible vertex functions [15,42–49] and the crossing of multiple solutions [41,45,46,48,50–53] of the Luttinger-Ward functional, with the local moment physics and its Kondo screening; (ii) the built-in limits of advanced perturbative approaches to describe these fundamental physical effects.

How to read two-particle quantities.—We start from the definition of the generalized local susceptibility [10,12,54]

$$\tilde{\chi}^{\nu\nu'}_{\sigma\sigma'}(\Omega) = G^{(2)}_{\sigma\sigma'}(\nu,\nu',\Omega) - T^{-1}G(\nu)G(\nu')\delta_{\Omega 0}\delta_{\sigma\sigma'} \quad (1)$$

in terms of the 2P ($G^{(2)}$) and 1P (G) Green's functions, where ν,ν' and Ω are fermionic and bosonic Matsubara frequencies, respectively, and $\sigma,\sigma' = \{\uparrow,\downarrow\}$ spin indices. As we show in the following for repulsive interactions, the generalized *charge* susceptibility $\tilde{\chi}^{\nu\nu'}(\Omega) = \tilde{\chi}^{\nu\nu'}_{\uparrow\uparrow}(\Omega) + \tilde{\chi}^{\nu\nu'}_{\uparrow\downarrow}(\Omega)$ allows for the best readability of the underlying physics at the 2P level. Furthermore, the physical response of this sector captures the fundamental properties of any interacting electron system. We recall that the physical response function (χ) is obtained from the generalized susceptibility $\tilde{\chi}^{\nu\nu'}(\Omega)$ by summing over the fermionic Matsubara frequencies ν,ν' [54]. The static charge response $\chi(\Omega = 0)$ reads

$$\chi = T^2\sum_{\nu\nu'}\tilde{\chi}^{\nu\nu'} = T^2\sum_{\nu\nu'}(\tilde{\chi}^{\nu\nu'}_{\uparrow\uparrow} + \tilde{\chi}^{\nu\nu'}_{\uparrow\downarrow}). \quad (2)$$

We start by analyzing the arguably simple case of an isolated atom with a repulsive interaction U (Hubbard atom, HA), where analytic expressions are also available [12,48]. This represents the purest realization of local moment physics, which hence provides an ideal baseline for the interpretation of the more interesting cases discussed below. In Fig. 1 (upper panels), we show an intensity plot of $\tilde{\chi}^{\nu\nu'}$ (normalized by T^2) for $U = 5.75$ [84], half filling (where $\tilde{\chi}^{\nu\nu'}$ is real [12,48]) and different temperatures. At high temperature ($T_{\text{high}} = 2$, left panel), the overall frequency structure consists of a large positive-valued diagonal (yellow and red) and a weak negative cross structure (blue). This corresponds to a typical *perturbative* behavior [12,16], dominated by the diagonal bubble term $\tilde{\chi}^{\nu\nu'}_0 = \tilde{\chi}^{\nu\nu'}_{0,\uparrow\uparrow} = -\delta_{\nu\nu'}G(\nu)^2/T$: Correlation effects are washed out for $T \gtrsim U$, consistent with the feasibility of high-T expansions.

The situation changes radically when reducing T: in the intermediate ($T_{\text{int}} = 0.1$) and low ($T_{\text{low}} = 1/60 \approx 0.017$) temperature regime (central and right panel), one observes a strong damping of all diagonal elements of $\tilde{\chi}^{\nu\nu'}$. The effect is more pronounced at low frequencies, as the sign of $\tilde{\chi}^{\nu=\nu'}$ becomes even *negative* (bluish colors) for $|\nu| \lesssim U$ [48] (black square). This major feature is accompanied by the appearance of small positive off-diagonal elements (yellow). The net effect is a suppression of the physical susceptibility χ, see Eq. (2), which occurs when the thermal energy is no longer large enough ($T \sim \nu < U$) to counter the formation of a local moment driven by U, eventually yielding an exponentially small $\chi \sim e^{-U/2T}$ for $T \to 0$. Altogether, the low-T HA results illustrate how the onset of a pure local moment is encoded in the charge sector: a progressive emergence of a nonperturbative sign structure in $\tilde{\chi}^{\nu\nu'}$, which is the opposite image of the perturbative one (left panel). This also induces several negative eigenvalues of $\tilde{\chi}^{\nu\nu'}$, responsible for the breakdown of perturbative expansions [41].

Let us now examine how this picture changes when the HA system is connected to an electronic bath (here: with a flat DOS of bandwidth $W = 20$ and hybridization $V = 2 < U = 5.75$ [84]), corresponding to the well-known Anderson impurity model (AIM). By comparing the results of $T^2\tilde{\chi}^{\nu\nu'}$ (central-row panels of Fig. 1, computed with w2dynamics [54]) to those of the HA, we observe almost no difference at T_{high}. This is not surprising as thermal fluctuations prevail over both correlation (U) and hybridization (V) effects in this case. Upon lowering T to T_{int}, we enter the local moment regime of the AIM. This is reflected in a qualitatively similar evolution as seen in the HA: a progressive suppression of the diagonal entries of $\tilde{\chi}^{\nu\nu'}$, turning negative in the low-energy sector (black square), accompanied by positive, yet smaller, off-diagonal contributions, with an overall freezing effect on the local density fluctuations [see Eq. (2) and the Supplemental Material [54]]. This is how the formation of a local moment affects the charge sector, thus representing its *fingerprint*. However, due to the screening effects of the bath its features get weakened, explaining the quantitative differences to the HA (e.g., the reduced size of the black square).

The most interesting situation is encountered when reducing T further down to $T_{\text{low}} \gtrsim T_K$ (right panel), where the Kondo screening induces qualitative differences with respect to the HA. We observe that the low-frequency diagonal elements of $\tilde{\chi}^{\nu\nu'}$ (white square) are flipped back to positive, as in the perturbative regime. This trend is driven by the low-energy correlations between electrons with antiparallel spins ($\tilde{\chi}^{\nu=\nu'}_{\uparrow\downarrow}$) [54]. The weakening of their negative contribution increases the physical charge susceptibility χ [see Eq. (2) and Supplemental Material [54]] and simultaneously mitigates the magnetic response. However, in the intermediate frequency regime, the diagonal elements of $\tilde{\chi}^{\nu\nu'}$ are still negative, reflecting the underlying presence of a (partially screened) local moment.

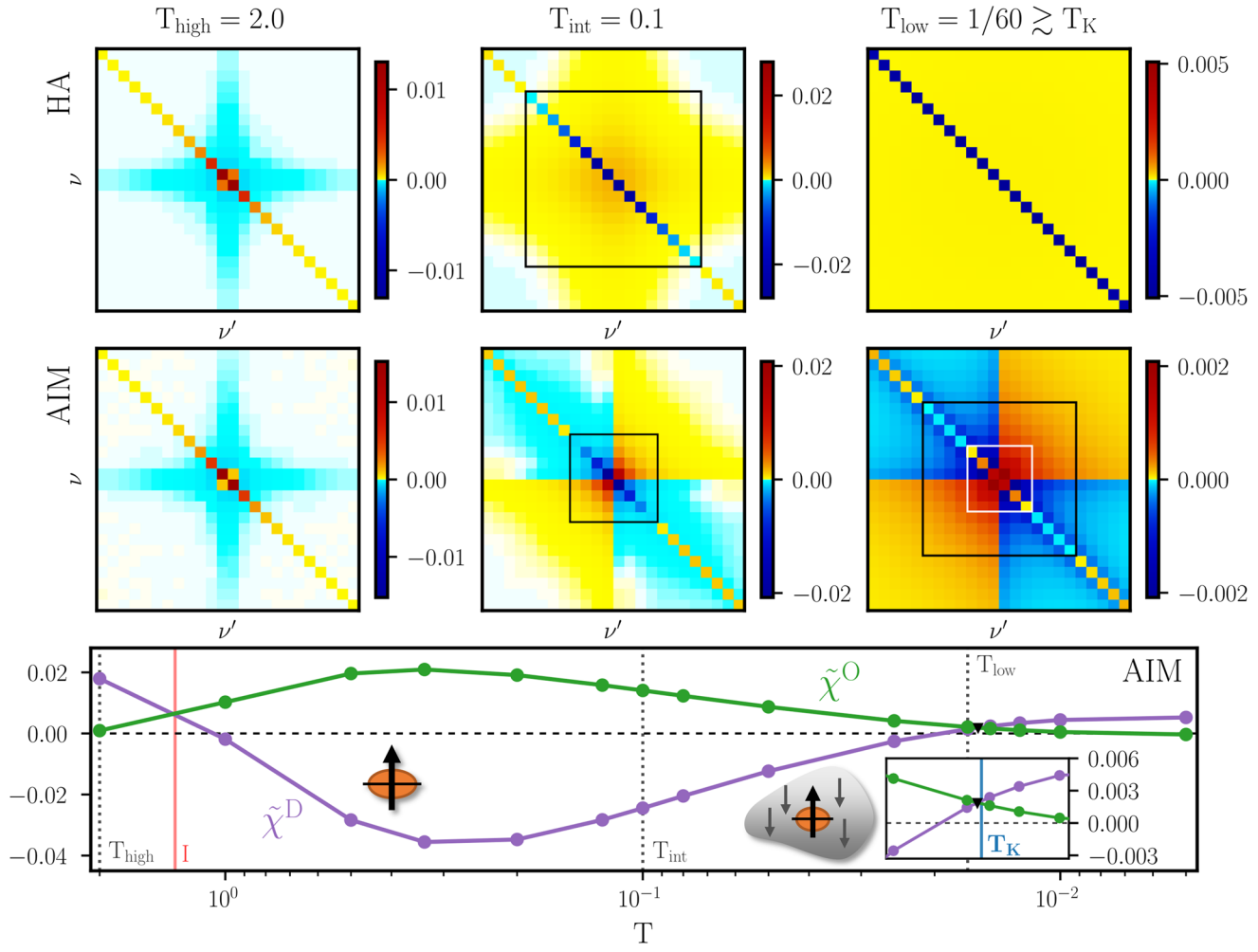

FIG. 1. Comparison of the Matsubara frequency structure of $T^2\tilde{\chi}^{\nu\nu'}(\Omega = 0)$ for the HA (top row) and the AIM (center row) for $U = 5.75$ [84] and different temperatures. The maximal Matsubara index is kept fixed for all temperatures (the labels are hidden to ensure better readability). Black and white squares mark the main frequency structures, as described in the text. Lower panel: Temperature evolution of the lowest Matsubara frequency elements of $T^2\tilde{\chi}^{\nu\nu'}(\Omega = 0)$: $\tilde{\chi}^D = T^2\tilde{\chi}^{\pi T,\pi T}$ (violet) and $\tilde{\chi}^O = T^2\tilde{\chi}^{\pi T,-\pi T}$ (green). They cross at T_{high} at the divergence of Γ (red, I), and at low-temperatures at $T \simeq T_K$ (black triangle), see also the inset showing a zoom around T_K (vertical blue line). The arrows with and without the surrounding cloud sketch the local moment and the Kondo screened regime, respectively.

The fingerprint of the Kondo regime is, thus, the *onionlike* frequency structure of $\tilde{\chi}^{\nu\nu'}$, which is clearly recognizable in the rightmost central panel of Fig. 1: (i) a high-frequency perturbative asymptotic, (ii) a local moment driven structure (with suppressed diagonal) at intermediate frequencies, (iii) an inner core [with a similar sign structure as (i)] induced by the Kondo screening. A quick glance at the sign structure of $\tilde{\chi}^{\nu\nu'}$ therefore allows for an immediate understanding of the underlying physics. This nicely illustrates the balanced competition in the charge sector between the freezing effects of the local moment and the defreezing effects of its low-energy screening, which characterizes the Kondo regime.

Note, that the onionlike structure is also found for other values of U, as well as in other models [54], discussed below.

How to extract the Kondo temperature.—The behavior described above is also reflected in the temperature evolution of the lowest frequency entries of $\tilde{\chi}^{\nu\nu'}$: the diagonal $\tilde{\chi}^D = T^2\tilde{\chi}^{\pi T,\pi T}$ and the off-diagonal $\tilde{\chi}^O = T^2\tilde{\chi}^{\pi T,-\pi T}$, shown in the lowest panel of Fig. 1. We can readily trace the sign changes marking the three regimes discussed above, associating the (negative) minimum of $\tilde{\chi}^D$ with the temperature at which the strongest local moment effects are observed. The screening induced enhancement of $\tilde{\chi}^D$ at lower temperatures has remarkable consequences: We find that crossing the Kondo temperature, as defined in a standard way from the behavior of the static magnetic response of the system [54] ($T_K = 1/65 \approx 0.015$ at $U = 5.75$ for the AIM), matches with high accuracy the equality of $\tilde{\chi}^D$ and $\tilde{\chi}^O$ observed at low-T (see inset of Fig. 1, marked by black triangle).

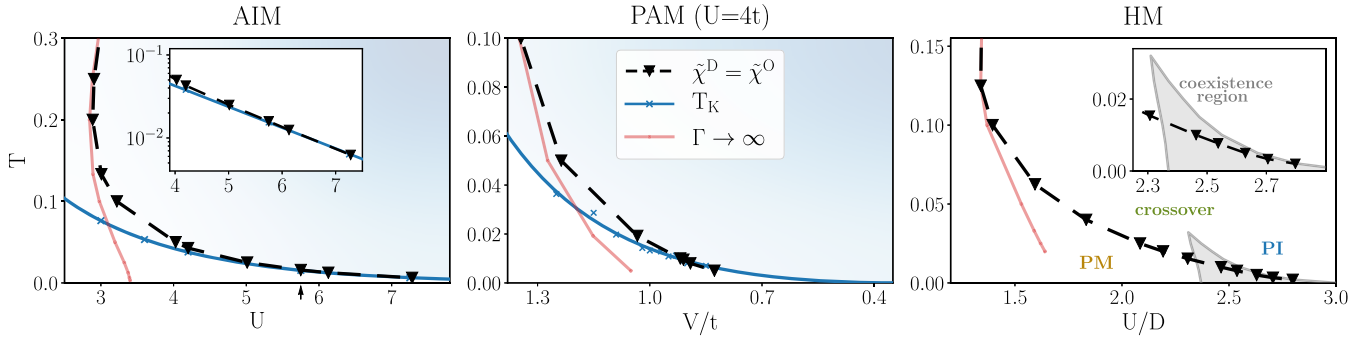

FIG. 2. Phase diagram of the AIM (left), the PAM (DMFT) (middle), and the HM (DMFT) (right) as a function of the interaction U (hybridization V for the PAM, U fixed) and the temperature T showing the line where $\tilde{\chi}^D = \tilde{\chi}^{\mathrm{O}}$ holds (black triangles, dashed), i.e., the singularity of the 2×2 submatrix of $\tilde{\chi}^{\nu\nu'}$. The left and central panels show the agreement at low temperatures between T_K (blue solid line) and the condition $\tilde{\chi}^D = \tilde{\chi}^{\mathrm{O}}$, clearly evident also in logarithmic scale (left inset). The local moment regime is represented by a bluish shadowed area in both panels. The red lines denote the (first) divergence of the irreducible vertex Γ. For the HM on the Bethe lattice the paramagnetic metallic (PM) and insulating (PI) phases are indicated together with their crossover. The coexistence region is shown in gray. The arrow on the abscissa (left) marks the interaction value used in Figs. 1 and 3.

We emphasize that this criterion holds more generally. As shown in the phase diagram of the AIM in Fig. 2 (left panel), the condition $\tilde{\chi}^D = \tilde{\chi}^{\mathrm{O}}$ (black triangles) perfectly traces T_K (blue line) [85] in the entire local moment regime $T, V < U$ (see also the logarithmic inset), i.e., where the definition of a Kondo scale is actually meaningful. Note that this is not the case for other criteria one could naturally think of, such as $\tilde{\chi}^D = -\tilde{\chi}^{\mathrm{O}}$ or $\tilde{\chi}^D = 0$ [54].

Moreover, our simple 2P definition of T_K holds also beyond the single impurity problem. In Fig. 2, we show DMFT calculations for the periodic Anderson model on a square lattice with nearest-neighboring hopping t (PAM, central) and for a Hubbard model on a Bethe lattice with unitary half-bandwidth D (HM, right) [54].

In particular, we observe that for the PAM, the *same matching* of the condition $\tilde{\chi}^D = \tilde{\chi}^{\mathrm{O}}$ (black triangles) and T_K [54,86,87] (blue line) is found in the local moment regime (i.e., when $V < t$, blue-shadowed area).

In the HM, the Kondo temperature characterizing the auxiliary AIM associated with the self-consistent DMFT solution, depends on the temperature itself: $T_K^{\mathrm{HM}}(T)$. Hence, $\tilde{\chi}^D = \tilde{\chi}^{\mathrm{O}}$ (black triangles) indicates that the temperature equals the effective Kondo temperature, i.e., $T_K^{\mathrm{HM}}(T) = T$. Physically, it is natural to relate this condition to the onset of low-energy electronic coherence: For all temperatures below the $\tilde{\chi}^D = \tilde{\chi}^{\mathrm{O}}$ condition, a conventional Fermi-liquid behavior of the physical response can be expected [e.g., $\rho(T) \propto T^2$, $c_V(T) \propto T$, etc. [1]]. This would also be consistent with the $\tilde{\chi}^D = \tilde{\chi}^{\mathrm{O}}$ condition approaching the Mott Hubbard metal-insulator transition (MIT) at $U_{\mathrm{MIT}}(T = 0) = U_{c2}$ in the low-T limit (see also recent DMFT studies of the physics in the proximity of the MIT [88,89]).

The equality of the elements of the innermost 2×2 submatrix of $\tilde{\chi}^{\nu\nu'}$ represents therefore a very simple, clear-cut criterion for determining T_K at the 2P level.

A nonperturbative Fermi liquid.—Beyond its physical relevance, our improved 2P understanding sheds light onto the nontrivial relation with the breakdown of perturbation theory [41]. At high T, where $\nu_0 = \pi T \gtrsim V, U, t$, the 2×2 submatrix encodes all relevant energy scales, the rest being nonsingular high-frequency asymptotics. In this case $\tilde{\chi}^D = \tilde{\chi}^{\mathrm{O}}$ corresponds to a singular eigenvalue of the *entire* $\tilde{\chi}^{\nu\nu'}$ and hence to a divergence of the irreducible vertex function $\Gamma^{\nu\nu'} = [\tilde{\chi}^{\nu\nu'}]^{-1} - [\tilde{\chi}_0^{\nu\nu'}]^{-1}$, specifically to the first (I) one encountered when reducing the temperature (red line in Figs. 1 and 2) [42,45,47–49]. For intermediate temperatures, the 2×2 submatrix is controlled by the local moment, leading to a strongly negative $\tilde{\chi}^D$ and negative eigenvalues of the submatrix (as in the HA case). At T_K the eigenvalue flips sign and one finds again $\tilde{\chi}^D > \tilde{\chi}^{\mathrm{O}}$ for $T \lesssim T_K$, as in the perturbative regime (see Fig. 1, lowest panel). Here, however, because of the onionlike structure of $\tilde{\chi}^{\nu\nu'}$, the positive definiteness (and thus the invertibility) is guaranteed only for an inner submatrix describing the Fermi liquid regime, but not for the full $\tilde{\chi}^{\nu\nu'}$. This explains why divergences of irreducible vertex functions can occur also at low temperatures [47] even in the presence of a Fermi liquid ground state. Indeed, such vertex divergences mark the distinction between a Fermi liquid in the weak-coupling and in the strong-coupling regime.

Limitations of perturbative approaches.—The direct link between the 2P fingerprints of local moments and vertex divergences, sets precise physical limitations for perturbative methods, where—per construction—Γ is finite [90]. Hence, the impact of the characteristic physics emerging from the magnetic sector onto the charge channel, cannot be described by perturbative methods. We substantiate this statement by considering two advanced perturbative schemes, the functional renormalization group (fRG) [9,54] and the parquet approximation (PA) [16,54,91–101]. The results obtained for the AIM

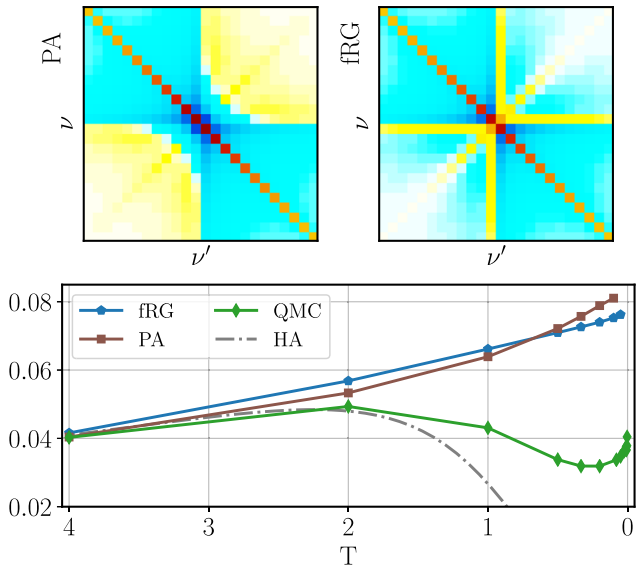

FIG. 3. Generalized charge susceptibility ($T^2\tilde{\chi}^{\nu\nu'}$) for the AIM, as obtained by means of PA and fRG for $U = 5.75$ and $T = T_{\text{int}}$. The same color scale as in Fig. 1 (AIM, T_{int}) is used. Lower panel: static physical charge susceptibility χ computed with different approaches as a function of T.

with $U = 5.75$ [84] and $T = T_{\text{int}}$ are shown in Fig. 3. $\tilde{\chi}^{\nu\nu'}$ computed by the fRG and PA (upper panels) appear qualitatively different from the (numerically) exact one of Fig. 1 (AIM, central): The diagonal elements are all *positive* and substantially larger than the off-diagonal ones. This ensures the positive definiteness of the entire $\tilde{\chi}^{\nu\nu'}$, preventing the suppression effects of the charge response, which characterize the local moment regime. This drawback qualitatively affects the physical description. In particular, the temperature dependence of the numerically exact physical charge susceptibility χ (Fig. 3, lower panel) exhibits a clear minimum for intermediate $T_{\text{high}} > T > T_K$. This emerges from the competition between the suppression induced by the local moment (see the extreme HA case) and the low-energy screening. Both features are *not* captured by the fRG (blue pentagons) and PA (brown squares), which display a monotonic behavior as T is decreased, in the framework of a mere thermal quenching. At the same time, the perturbative approaches are able to capture the qualitative correct behavior of the magnetic response, reflecting the absence of divergences of Γ in this sector [54].

Conclusions.—We have shown how fundamental physical properties of correlated systems, i.e., the local moment formation and its Kondo screening, can be directly read from the Matsubara frequency structure of the generalized *charge* susceptibility $\tilde{\chi}^{\nu\nu'}$. In particular, the competition between localization effects at higher energies and metallic screening at lower energies is encoded in a clearly recognizable "onionlike" fingerprint of $\tilde{\chi}^{\nu\nu'}$, emerging in the Kondo regime. The thorough inspection of the latter even discloses an alternative route to extract T_K from the charge sector. Our improved understanding of the 2P processes sets also clear-cut limits to the physics accessible to perturbative approaches.

As a future perspective, it will be worth to overcome the on-site and/or single-orbital framework of our study. We expect that the role of the local moments will be played by short-range [8,14,102,103] or Hund's-driven [104–106] magnetic fluctuations. Their nonperturbative images could reverberate, analogously as presented here, onto the charge and/or pairing response of the system. The identification of the corresponding fingerprints may open new pathways toward a microscopic understanding of unconventional superconductivity in the nonperturbative regime.

We thank M. Capone, S. Ciuchi, J. von Delft, K. Held, C. Hille, A. A. Katanin, F. Krien, F. B. Kugler, E. van Loon, C. Schattauer, and G. Sangiovanni for insightful discussions. The authors also want to thank the CCQ of the Flatiron Institute (Simons Foundation) for the great hospitality. The present work was supported by the Austrian Science Fund (FWF) through the Project No. I 2794-N35 (P. C., A. T.) and Erwin-Schrödinger Fellowship J 4266—"Superconductivity in the vicinity of Mott insulators" (SuMo, T. S.), the Deutsche Forschungsgemeinschaft (DFG) through Project No. AN 815/6-1 (S. A.), as well as the European Research Council for the European Union Seventh Framework Program (FP7/2007-2013) with ERC Grant No. 319286 (QMAC, T. S.).

[1] A. A. Abrikosov, L. P. Gorkov, and I. E. Dzyaloshinski, *Methods of Quantum Field Theory in Statistical Physics* (Dover, New York, 1975).
[2] G. D. Mahan, *Many-Particle Physics* (Kluwer Academic/Plenum Publishers, New York, 2000).
[3] A. Damascelli, Z. Hussain, and Z.-X. Shen, Angle-resolved photoemission studies of the cuprate superconductors, Rev. Mod. Phys. **75**, 473 (2003).
[4] G. Binnig and H. Rohrer, Scanning tunneling microscopy—from birth to adolescence, Rev. Mod. Phys. **59**, 615 (1987).
[5] O. Fischer, M. Kugler, I. Maggio-Aprile, C. Berthod, and C. Renner, Scanning tunneling spectroscopy of high-temperature superconductors, Rev. Mod. Phys. **79**, 353 (2007).
[6] S. M. Hayden, Neutron scattering and the magnetic response of superconductors and related compounds, in *Superconductivity: Conventional and Unconventional Superconductors*, edited by K. H. Bennemann and J. B. Ketterson (Springer, Berlin, Heidelberg, 2008), pp. 993–1029.
[7] D. C. Johnston, The puzzle of high temperature superconductivity in layered iron pnictides and chalcogenides, Adv. Phys. **59**, 803 (2010).
[8] T. Maier, M. Jarrell, T. Pruschke, and M. H. Hettler, Quantum cluster theories, Rev. Mod. Phys. **77**, 1027 (2005).

[9] W. Metzner, M. Salmhofer, C. Honerkamp, V. Meden, and K. Schönhammer, Functional renormalization group approach to correlated fermion systems, Rev. Mod. Phys. **84**, 299 (2012).
[10] G. Rohringer, H. Hafermann, A. Toschi, A. A. Katanin, A. E. Antipov, M. I. Katsnelson, A. I. Lichtenstein, A. N. Rubtsov, and K. Held, Diagrammatic routes to nonlocal correlations beyond dynamical mean field theory, Rev. Mod. Phys. **90**, 025003 (2018).
[11] J. Kuneš, Efficient treatment of two-particle vertices in dynamical mean-field theory, Phys. Rev. B **83**, 085102 (2011).
[12] G. Rohringer, A. Valli, and A. Toschi, Local electronic correlation at the two-particle level, Phys. Rev. B **86**, 125114 (2012).
[13] H. Hafermann, Self-energy and vertex functions from hybridization-expansion continuous-time quantum Monte Carlo for impurity models with retarded interaction, Phys. Rev. B **89**, 235128 (2014).
[14] O. Gunnarsson, T. Schäfer, J. P. F. LeBlanc, E. Gull, J. Merino, G. Sangiovanni, G. Rohringer, and A. Toschi, Fluctuation Diagnostics of the Electron Self-Energy: Origin of the Pseudogap Physics, Phys. Rev. Lett. **114**, 236402 (2015).
[15] O. Gunnarsson, T. Schäfer, J. P. F. LeBlanc, J. Merino, G. Sangiovanni, G. Rohringer, and A. Toschi, Parquet decomposition calculations of the electronic self-energy, Phys. Rev. B **93**, 245102 (2016).
[16] N. Wentzell, G. Li, A. Tagliavini, C. Taranto, G. Rohringer, K. Held, A. Toschi, and S. Andergassen, High-frequency asymptotics of the vertex function: Diagrammatic parametrization and algorithmic implementation, Phys. Rev. B **102**, 085106 (2020).
[17] J. Kaufmann, P. Gunacker, and K. Held, Continuous-time quantum Monte Carlo calculation of multiorbital vertex asymptotics, Phys. Rev. B **96**, 035114 (2017).
[18] F. B. Kugler and J. von Delft, Multiloop functional renormalization group for general models, Phys. Rev. B **97**, 035162 (2018).
[19] A. Tagliavini, S. Hummel, N. Wentzell, S. Andergassen, A. Toschi, and G. Rohringer, Efficient Bethe-Salpeter equation treatment in dynamical mean-field theory, Phys. Rev. B **97**, 235140 (2018).
[20] E. A. Stepanov, S. Brener, F. Krien, M. Harland, A. I. Lichtenstein, and M. I. Katsnelson, Effective Heisenberg Model and Exchange Interaction for Strongly Correlated Systems, Phys. Rev. Lett. **121**, 037204 (2018).
[21] E. G. C. P. van Loon, F. Krien, H. Hafermann, A. I. Lichtenstein, and M. I. Katsnelson, Fermion-boson vertex within dynamical mean-field theory, Phys. Rev. B **98**, 205148 (2018).
[22] F. B. Kugler and J. von Delft, Derivation of exact flow equations from the self-consistent parquet relations, New J. Phys. **20**, 123029 (2018).
[23] E. A. Stepanov, A. Huber, A. I. Lichtenstein, and M. I. Katsnelson, Effective Ising model for correlated systems with charge ordering, Phys. Rev. B **99**, 115124 (2019).
[24] F. Krien, A. Valli, and M. Capone, Single-boson exchange decomposition of the vertex function, Phys. Rev. B **100**, 155149 (2019).
[25] E. A. Stepanov, V. Harkov, and A. I. Lichtenstein, Consistent partial bosonization of the extended Hubbard model, Phys. Rev. B **100**, 205115 (2019).
[26] F. Krien and A. Valli, Parquetlike equations for the Hedin three-leg vertex, Phys. Rev. B **100**, 245147 (2019).
[27] C. Hille, F. B. Kugler, C. J. Eckhardt, Y.-Y. He, A. Kauch, C. Honerkamp, A. Toschi, and S. Andergassen, Quantitative functional renormalization group description of the two-dimensional Hubbard model, Phys. Rev. Research **2**, 033372 (2020).
[28] E. G. C. P. van Loon, F. Krien, and A. A. Katanin, Bethe-Salpeter Equation at the Critical End Point of the Mott Transition, Phys. Rev. Lett. **125**, 136402 (2020).
[29] M. Reitner, P. Chalupa, L. Del Re, D. Springer, S. Ciuchi, G. Sangiovanni, and A. Toschi, Attractive Effect of a Strong Electronic Repulsion: The Physics of Vertex Divergences, Phys. Rev. Lett. **125**, 196403 (2020).
[30] F. B. Kugler, S-S. B. Lee, and J. von Delft, Multipoint correlation functions: spectral representation and numerical evaluation, arXiv:2101.00707.
[31] S-S. B. Lee, F. B. Kugler, J. von Delft, Computing local multipoint correlators using the numerical renormalization group, arXiv:2101.00708
[32] F. Krien, E. G. C. P. van Loon, M. I. Katsnelson, A. I. Lichtenstein, and M. Capone, Two-particle Fermi liquid parameters at the Mott transition: Vertex divergences, Landau parameters, and incoherent response in dynamical mean-field theory, Phys. Rev. B **99**, 245128 (2019).
[33] C. Melnick and G. Kotliar, Fermi-liquid theory and divergences of the two-particle irreducible vertex in the periodic Anderson lattice, Phys. Rev. B **101**, 165105 (2020).
[34] A. Hewson, *The Kondo Problem to Heavy Fermions* (Cambridge University Press, Cambridge, England, 1993).
[35] Z. Fisk, D. W. Hess, C. J. Pethick, D. Pines, J. L. Smith, J. D. Thompson, and J. O. Willis, Heavy-electron metals: New highly correlated states of matter, Science **239**, 33 (1988).
[36] E. Dagotto, Correlated electrons in high-temperature superconductors, Rev. Mod. Phys. **66**, 763 (1994).
[37] P. A. Lee, N. Nagaosa, and X.-G. Wen, Doping a Mott insulator: Physics of high-temperature superconductivity, Rev. Mod. Phys. **78**, 17 (2006).
[38] P. Coleman, Heavy fermions: Electrons at the edge of magnetism, in *Handbook of Magnetism and Advanced Magnetic Materials*, edited by H. Kronmuller and S. Parkin, Vol. 1, Fundamentals and Theory (John Wiley and Sons, New York, 2007).
[39] S. Andergassen, V. Meden, H. Schoeller, J. Splettstoesser, and M. R. Wegewijs, Charge transport through single molecules, quantum dots and quantum wires, Nanotechnology **21**, 272001 (2010).
[40] A. Georges, G. Kotliar, W. Krauth, and M. J. Rozenberg, Dynamical mean-field theory of strongly correlated fermion systems and the limit of infinite dimensions, Rev. Mod. Phys. **68**, 13 (1996).
[41] O. Gunnarsson, G. Rohringer, T. Schäfer, G. Sangiovanni, and A. Toschi, Breakdown of Traditional Many-Body Theories for Correlated Electrons, Phys. Rev. Lett. **119**, 056402 (2017).

[42] T. Schäfer, G. Rohringer, O. Gunnarsson, S. Ciuchi, G. Sangiovanni, and A. Toschi, Divergent Precursors of the Mott-Hubbard Transition at the Two-Particle Level, Phys. Rev. Lett. **110**, 246405 (2013).
[43] V. Janiš and V. Pokorný, Critical metal-insulator transition and divergence in a two-particle irreducible vertex in disordered and interacting electron systems, Phys. Rev. B **90**, 045143 (2014).
[44] T. Ribic, G. Rohringer, and K. Held, Nonlocal correlations and spectral properties of the Falicov-Kimball model, Phys. Rev. B **93**, 195105 (2016).
[45] T. Schäfer, S. Ciuchi, M. Wallerberger, P. Thunström, O. Gunnarsson, G. Sangiovanni, G. Rohringer, and A. Toschi, Nonperturbative landscape of the Mott-Hubbard transition: Multiple divergence lines around the critical endpoint, Phys. Rev. B **94**, 235108 (2016).
[46] J. Vučičević, N. Wentzell, M. Ferrero, and O. Parcollet, Practical consequences of the Luttinger-Ward functional multivaluedness for cluster DMFT methods, Phys. Rev. B **97**, 125141 (2018).
[47] P. Chalupa, P. Gunacker, T. Schäfer, K. Held, and A. Toschi, Divergences of the irreducible vertex functions in correlated metallic systems: Insights from the Anderson impurity model, Phys. Rev. B **97**, 245136 (2018).
[48] P. Thunström, O. Gunnarsson, S. Ciuchi, and G. Rohringer, Analytical investigation of singularities in two-particle irreducible vertex functions of the Hubbard atom, Phys. Rev. B **98**, 235107 (2018).
[49] D. Springer, P. Chalupa, S. Ciuchi, G. Sangiovanni, and A. Toschi, Interplay between local response and vertex divergences in many-fermion systems with on-site attraction, Phys. Rev. B **101**, 155148 (2020).
[50] E. Kozik, M. Ferrero, and A. Georges, Nonexistence of the Luttinger-Ward Functional and Misleading Convergence of Skeleton Diagrammatic Series for Hubbard-Like Models, Phys. Rev. Lett. **114**, 156402 (2015).
[51] A. Stan, P. Romaniello, S. Rigamonti, L. Reining, and J. A. Berger, Unphysical and physical solutions in many-body theories: From weak to strong correlation, New J. Phys. **17**, 093045 (2015).
[52] W. Tarantino, B. S. Mendoza, P. Romaniello, J. A. Berger, and L. Reining, Many-body perturbation theory and non-perturbative approaches: Screened interaction as the key ingredient, J. Phys. Condens. Matter **30**, 135602 (2018).
[53] A. J. Kim, P. Werner, and E. Kozik, Strange metal solution in the diagrammatic theory for the 2*d* Hubbard model, arXiv:2012.06159
[54] See Supplemental Material at http://link.aps.org/supplemental/10.1103/PhysRevLett.126.056403 for general definitions and specifics on the numerical methods, including the calculation of the Kondo temperature, as well as further details on the frequency structures of the generalized susceptibility and limitations of the perturbative approaches, which includes Refs. [52–80].
[55] M. Wallerberger, A. Hausoel, P. Gunacker, A. Kowalski, N. Parragh, F. Goth, K. Held, and G. Sangiovanni, w2dynamics: Local one- and two-particle quantities from dynamical mean field theory, Comput. Phys. Commun. **235**, 388 (2019).
[56] E. Gull, A. J. Millis, A. I. Lichtenstein, A. N. Rubtsov, M. Troyer, and P. Werner, Continuous-time Monte Carlo methods for quantum impurity models, Rev. Mod. Phys. **83**, 349 (2011).
[57] H. R. Krishna-murthy, K. G. Wilson, and J. W. Wilkins, Temperature-Dependent Susceptibility of the Symmetric Anderson Model: Connection to the Kondo Model, Phys. Rev. Lett. **35**, 1101 (1975).
[58] H. R. Krishna-murthy, J. W. Wilkins, and K. G. Wilson, Renormalization-group approach to the Anderson model of dilute magnetic alloys. I. Static properties for the symmetric case, Phys. Rev. B **21**, 1003 (1980).
[59] A. Tagliavini, C. Hille, F. Kugler, S. Andergassen, A. Toschi, and C. Honerkamp, Multiloop functional renormalization group for the two-dimensional Hubbard model: Loop convergence of the response functions, SciPost Phys. **6**, 009 (2019).
[60] S. Andergassen, T. Enss, and V. Meden, Kondo physics in transport through a quantum dot with Luttinger-liquid leads, Phys. Rev. B **73**, 153308 (2006).
[61] L. Bartosch, H. Freire, J. J. R. Cardenas, and P. Kopietz, A functional renormalization group approach to the Anderson impurity model, J. Phys. Condens. Matter **21**, 305602 (2009).
[62] C. Karrasch, A. Oguri, and V. Meden, Josephson current through a single Anderson impurity coupled to BCS leads, Phys. Rev. B **77**, 024517 (2008).
[63] A. Eichler, R. Deblock, M. Weiss, C. Karrasch, V. Meden, C. Schönenberger, and H. Bouchiat, Tuning the Josephson current in carbon nanotubes with the Kondo effect, Phys. Rev. B **79**, 161407(R) (2009).
[64] R. Gezzi, T. Pruschke, and V. Meden, Functional renormalization group for nonequilibrium quantum many-body problems, Phys. Rev. B **75**, 045324 (2007).
[65] R. Hedden, V. Meden, T. Pruschke, and K. Schönhammer, A functional renormalization group approach to zero-dimensional interacting systems, J. Phys. Condens. Matter **16**, 5279 (2004).
[66] A. Isidori, D. Roosen, L. Bartosch, W. Hofstetter, and P. Kopietz, Spectral function of the Anderson impurity model at finite temperatures, Phys. Rev. B **81**, 235120 (2010).
[67] S. G. Jakobs, M. Pletyukhov, and H. Schoeller, Nonequilibrium functional renormalization group with frequency-dependent vertex function: A study of the single-impurity Anderson model, Phys. Rev. B **81**, 195109 (2010).
[68] C. Karrasch, T. Enss, and V. Meden, Functional renormalization group approach to transport through correlated quantum dots, Phys. Rev. B **73**, 235337 (2006).
[69] C. Karrasch, T. Hecht, A. Weichselbaum, Y. Oreg, J. von Delft, and V. Meden, Mesoscopic to Universal Crossover of the Transmission Phase of Multilevel Quantum Dots, Phys. Rev. Lett. **98**, 186802 (2007).
[70] C. Karrasch, T. Hecht, A. Weichselbaum, J. von Delft, Y. Oreg, and V. Meden, Phase lapses in transmission through interacting two-level quantum dots, New J. Phys. **9**, 123 (2007).
[71] C. Karrasch, R. Hedden, R. Peters, T. Pruschke, K. Schönhammer, and V. Meden, A finite-frequency functional renormalization group approach to the single

impurity Anderson model, J. Phys. Condens. Matter **20**, 345205 (2008).
[72] C. Karrasch and V. Meden, Supercurrent and multiple singlet-doublet phase transitions of a quantum dot Josephson junction inside an Aharonov-Bohm ring, Phys. Rev. B **79**, 045110 (2009).
[73] V. Kashcheyevs, C. Karrasch, T. Hecht, A. Weichselbaum, V. Meden, and A. Schiller, Quantum Criticality Perspective on the Charging of Narrow Quantum-Dot Levels, Phys. Rev. Lett. **102**, 136805 (2009).
[74] H. Schmidt and P. Wölfle, Transport through a Kondo quantum dot: Functional RG approach, Ann. Phys. (Amsterdam) **19**, 60 (2010).
[75] M. Weyrauch and D. Sibold, Transport through correlated quantum dots using the functional renormalization group, Phys. Rev. B **77**, 125309 (2008).
[76] C. Karrasch, M. Pletyukhov, L. Borda, and V. Meden, Functional renormalization group study of the interacting resonant level model in and out of equilibrium, Phys. Rev. B **81**, 125122 (2010).
[77] A. A. Katanin, Fulfillment of Ward identities in the functional renormalization group approach, Phys. Rev. B **70**, 115109 (2004).
[78] P. Chalupa, C. Hille, F. B. Kugler, J. von Delft, S. Andergassen, and A. Toschi (2020) (to be published).
[79] C. De Dominicis and P. C. Martin, Stationary entropy principle and renormalization in normal and superfluid systems. I. Algebraic formulation, J. Math. Phys. (N.Y.) **5**, 14 (1964).
[80] C. De Dominicis and P. C. Martin, Stationary entropy principle and renormalization in normal and superfluid systems. II. Diagrammatic formulation, J. Math. Phys. (N.Y.) **5**, 31 (1964).
[81] V. Janiš, Stability of self-consistent solutions for the Hubbard model at intermediate and strong coupling, Phys. Rev. B **60**, 11345 (1999).
[82] C. Taranto, S. Andergassen, J. Bauer, K. Held, A. Katanin, W. Metzner, G. Rohringer, and A. Toschi, From Infinite to Two Dimensions Through the Functional Renormalization Group, Phys. Rev. Lett. **112**, 196402 (2014).
[83] D. Vilardi, C. Taranto, and W. Metzner, Antiferromagnetic and d-wave pairing correlations in the strongly interacting two-dimensional Hubbard model from the functional renormalization group, Phys. Rev. B **99**, 104501 (2019).
[84] The value of $U = 5.75$ has been chosen such that the local moment is already well defined and, at the same time, calculations are still feasible within PA and fRG, allowing for direct comparisons. Similar results are obtained for other U's, see Supplemental Material [54]. For the AIM the interaction is often compared to $\Delta = V^2\pi\rho_0$. In our case $\rho_0 = (1/W)$ and $\Delta = \pi/5$, hence $U/\Delta \approx 9.15$.
[85] For different interaction values T_K is extracted [54] (blue crosses), and then fitted using an analytical expression for T_K in the wide-band limit [34] $[A\sqrt{U\Delta}\exp[-B(U/\Delta) + C(\Delta/U)]]$.
[86] T. Schäfer, A. A. Katanin, M. Kitatani, A. Toschi, and K. Held, Quantum Criticality in the Two-Dimensional Periodic Anderson Model, Phys. Rev. Lett. **122**, 227201 (2019).
[87] G. Rohringer, A. Katanin, T. Schäfer, A. Hausoel, K. Held, and A. Toschi, LadderDΓA code, github.com/ladderDGA (2018).
[88] H. Terletska, J. Vučičević, D. Tanasković, and V. Dobrosavljević, Quantum Critical Transport Near the Mott Transition, Phys. Rev. Lett. **107**, 026401 (2011).
[89] J. Vučičević, H. Terletska, D. Tanasković, and V. Dobrosavljević, Finite-temperature crossover and the quantum Widom line near the Mott transition, Phys. Rev. B **88**, 075143 (2013).
[90] With the only exception of second-order phase transitions to long-range ordered phases, not relevant here.
[91] *Theoretical Methods for Strongly Correlated Electrons*, edited by D. Sénéchal, A.-M. Tremblay, and C. Bourbonnais (Springer-Verlag, New York, Berlin, Heidelberg, 2004), pp. 237–296.
[92] V. Janiš and P. Augustinský, Analytic impurity solver with Kondo strong-coupling asymptotics, Phys. Rev. B **75**, 165108 (2007).
[93] V. Janiš and P. Augustinský, Kondo behavior in the asymmetric Anderson model: Analytic approach, Phys. Rev. B **77**, 085106 (2008).
[94] S. X. Yang, H. Fotso, J. Liu, T. A. Maier, K. Tomko, E. F. D'Azevedo, R. T. Scalettar, T. Pruschke, and M. Jarrell, Parquet approximation for the 4×4 Hubbard cluster, Phys. Rev. E **80**, 046706 (2009).
[95] K.-M. Tam, H. Fotso, S.-X. Yang, T.-W. Lee, J. Moreno, J. Ramanujam, and M. Jarrell, Solving the parquet equations for the Hubbard model beyond weak coupling, Phys. Rev. E **87**, 013311 (2013).
[96] A. Valli, T. Schäfer, P. Thunström, G. Rohringer, S. Andergassen, G. Sangiovanni, K. Held, and A. Toschi, Dynamical vertex approximation in its parquet implementation: Application to Hubbard nanorings, Phys. Rev. B **91**, 115115 (2015).
[97] G. Li, N. Wentzell, P. Pudleiner, P. Thunström, and K. Held, Efficient implementation of the parquet equations: Role of the reducible vertex function and its kernel approximation, Phys. Rev. B **93**, 165103 (2016).
[98] V. Janiš, P. Zalom, V. Pokorný, and A. Klíč, Strongly correlated electrons: Analytic mean-field theories with two-particle self-consistency, Phys. Rev. B **100**, 195114 (2019).
[99] V. Janiš and A. Klíč, Kondo temperature and high to low temperature crossover in impurity models of correlated electrons, JPS Conf. Proc. **30**, 011124 (2020).
[100] A. Kauch, P. Pudleiner, K. Astleithner, P. Thunström, T. Ribic, and K. Held, Generic Optical Excitations of Correlated Systems: π-Tons, Phys. Rev. Lett. **124**, 047401 (2020).
[101] V. Janiš, A. Klíč, J. Yan, and V. Pokorný, Curie-Weiss susceptibility in strongly correlated electron systems, Phys. Rev. B **102**, 205120 (2020).
[102] G. Sordi, K. Haule, and A. M. S. Tremblay, Finite Doping Signatures of the Mott Transition in the Two-Dimensional Hubbard Model, Phys. Rev. Lett. **104**, 226402 (2010).
[103] G. Sordi, P. Sémon, K. Haule, and A.-M. S. Tremblay, Strong Coupling Superconductivity, Pseudogap, and Mott Transition, Phys. Rev. Lett. **108**, 216401 (2012).

[104] K. Haule and G. Kotliar, Coherence-incoherence crossover in the normal state of iron oxypnictides and importance of Hund's rule coupling, New J. Phys. **11**, 025021 (2009).

[105] L. de' Medici, J. Mravlje, and A. Georges, Janus-Faced Influence of Hund's Rule Coupling in Strongly Correlated Materials, Phys. Rev. Lett. **107**, 256401 (2011).

[106] A. Chubukov and P. J. Hirschfeld, Iron-based superconductors, seven years later, Phys. Today **68**, 6, 46 (2015).